Circular RNA-ZNF532 regulates diabetes-induced retinal pericyte degeneration and vascular dysfunction

Qin Jiang,[1,2] Chang Liu,[2] Chao-Peng Li,[3] Shan-Shan Xu,[2] Mu-Di Yao,[2] Hui-Min Ge,[1,2] Ya-Nan Sun,[4] Xiu-Miao Li,[1] Shu-Jie Zhang,[4] Kun Shan,[4] Bai-Hui Liu,[4] Jin Yao,[1,2] Chen Zhao,[4,5,6] and Biao Yan[4,5,6]

[1]Affiliated Eye Hospital and [2]Fourth School of Clinical Medicine, Nanjing Medical University, Nanjing, China. [3]Department of Ophthalmology, Huai'an First People's Hospital, Huai An, China. [4]Eye Institute, Eye and ENT Hospital, Shanghai Medical College, Fudan University, Shanghai, China. [5]Shanghai Key Laboratory of Visual Impairment and Restoration, Shanghai, China. [6]National Health Commission (NHC) Key Laboratory of Myopia, Fudan University, Shanghai, China.

Diabetic retinopathy (DR) is the leading cause of blindness in working-age adults. Vascular pericyte degeneration is the predominant clinical manifestation of DR, yet the mechanism governing pericyte degeneration is poorly understood. Circular RNAs (circRNAs) play important roles in multiple biological processes and disease progression. Here, we investigated the role of circRNA in pericyte biology and diabetes-induced retinal vascular dysfunction. cZNF532 expression was upregulated in pericytes under diabetic stress, in the retinal vessels of a diabetic murine model, and in the vitreous humor of diabetic patients. cZNF532 silencing reduced the viability, proliferation, and differentiation of pericytes and suppressed the recruitment of pericytes toward endothelial cells in vitro. cZNF532 regulated pericyte biology by acting as a miR-29a-3p sponge and inducing increased expression of NG2, LOXL2, and CDK2. Knockdown of cZNF532 or overexpression of miR-29a-3p aggravated streptozotocin-induced retinal pericyte degeneration and vascular dysfunction. By contrast, overexpression of cZNF532 or inhibition of miR-29a-3p ameliorated human diabetic vitreous–induced retinal pericyte degeneration and vascular dysfunction. Collectively, these data identify a circRNA-mediated mechanism that coordinates pericyte biology and vascular homeostasis in DR. Induction of cZNF532 or antagonism of miR-29a-3p is an exploitable therapeutic approach for the treatment of DR.

Introduction

Pericytes are found on almost all capillaries as well as on small arterioles and venules throughout the body. They are embedded within the basement membranes and wrap endothelial cells to establish strong physical contacts (1, 2). Pericytes are important regulators of vascular development, angiogenesis, and vascular stabilization (3, 4). Pericyte degeneration has been observed in a series of human disorders, such as diabetic microvascular complications, tissue fibrosis, and cancers (5–7). Despite the pivotal role of pericyte in biological processes and human disorders, the mechanism governing pericyte biology remains largely unknown.

Diabetes-associated vascular complications are the major causes of morbidity and mortality among diabetic patients. Diabetic retinopathy (DR) is the most common microvascular complication of diabetes (8, 9). Of note, pericyte degeneration is considered the early hallmark of diabetes-induced retinal vascular dysfunction. Pericyte coverage is obviously greater in retinal capillaries than in other capillaries (10, 11). Moreover, retinal capillaries can be observed directly and noninvasively, providing an excellent system for studying pericyte biology (12). The mechanisms that govern pericyte biology have been investigated. Aberrant Angiopoietin-1/Tie2 signaling, platelet-derived growth factor (PDGF) signaling, or transforming growth factor (TGF) signaling can induce pericyte degeneration in retinal capillaries (13–16). However, there is extensive overlap and complex crosstalk among these signaling pathways. A new insight into the mechanism that drives pericyte degeneration may provide a novel therapeutic strategy for DR.

Circular RNAs (circRNAs) are a novel type of endogenous noncoding RNAs with closed-loop structures, which are broadly expressed in the eukaryotic transcriptome (17, 18). circRNAs usually display a tissue-specific or developmental-specific expression pattern. They regulate gene expression by acting as microRNA sponges or the regulators of parental gene transcription or alternative splicing (19). Aberrant circRNA expression has been reported in many human diseases, including cancers, neurodegeneration, and cardiovascular diseases (20, 21). In this study, we investigated the role of circRNAs in pericyte degeneration and diabetes-induced retinal dysfunction. We showed that overexpression of cZNF532 or inhibition of miR-29a-3p ameliorated diabetes-induced pericyte degeneration and retinal vascular dysfunction. Thus, the intervention of cZNF532-mediated signaling offers a promising opportunity for the treatment of DR.

Results

Identification of cZNF532 as a high glucose–regulated circRNA in pericytes. To identify high glucose–regulated circRNAs, we incubated human retinal pericytes with 5.55 mM glucose (normal glucose, NG), 5.55 mM glucose plus 24.45 mM pyruvate (osmotic control, OS), or 30 mM glucose (high glucose, HG) for 24 hours, and then prepared RNA samples for circRNA expression profiles.

Authorship note: QJ, CL, CPL, SSX, MDY, and HMG contributed equally to this work.
Conflict of interest: The authors have declared that no conflict of interest exists.

Submitted: July 6, 2018; **Accepted:** April 22, 2020; **Published:** June 15, 2020.
Reference information: *J Clin Invest*. 2020;130(7):3833–3847.
https://doi.org/10.1172/JCI123353.

One-way analysis of variance (ANOVA) was conducted to identify differentially expressed circRNAs among the HG, NG, and OS groups. We set the threshold as fold change over 2.0 and *P* value under 0.05, and identified 1523 differentially expressed circRNAs between the HG group and NG group (625 upregulated and 898 downregulated, Supplemental Data Set 1; supplemental material available online with this article; https://doi.org/10.1172/JCI123353DS1) and 792 circRNAs between the HG group and OS group (386 upregulated and 406 downregulated, Supplemental Data Set 2). Venn diagrams were generated to identify high glucose–regulated circRNAs and exclude osmotic pressure–regulated circRNAs. Eighty-six upregulated and 97 downregulated circRNAs were specifically regulated by high glucose (Supplemental Data Set 3 and Supplemental Figure 1A). Hierarchical clustering analysis of high glucose–regulated circRNAs divided the samples into 3 groups, showing a clear switch among HG, NG, and OS groups (Supplemental Figure 1B). We then conducted real-time reverse transcription PCR (qRT-PCR) to detect the expression pattern of 5 upregulated and 5 downregulated circRNAs identified by circRNA microarray. Expression of circ_0047814, circ_0001757, circ_0002085, circ_0002404, or circ_0004588 was upregulated by the treatment of pericytes with 30 mM glucose. By contrast, the expression of circ_0090921, circ_0086414, circ_0084156, circ_0084062, or circ_0082423 expression was downregulated in response to 30 mM glucose (Supplemental Figure 1C).

Of these verified circRNAs, circ_0047814 was the most upregulated circRNA. It had a homologous gene in mouse genome (mmu_circ_0000883) and the sequence similarity was over 85%, which was suitable for determining its biological function using the mouse model. circ_0047814 was named cZNF532 because its host gene was ZNF532. Sanger sequencing confirmed that cZNF532 expression was constitutively expressed in retinal pericytes (Figure 1A). cZNF532 was resistant to RNAse R digestion, whereas linear ZNF532 mRNA was easily degraded (Figure 1B). qRT-PCR revealed that cZNF532 was mainly expressed in the cytoplasm of pericytes (Figure 1C).

We further determined whether diabetic stress influenced cZNF532 expression in vivo and in vitro. Streptozotocin (STZ) was administered to 8-week-old C57BL/6J mice over 5 consecutive days to build a diabetic murine model. Retinal vessels were extracted from the retinas at 1 month, 2 months, 4 months, and 6 months after induction of diabetes using anti–mouse CD31 antibody, followed by sheep anti–mouse IgG–conjugated magnetic beads and magnetic separation (22). cZNF532 expression was significantly upregulated in diabetic vessels compared with nondiabetic controls (Figure 1D). Human retinal pericytes or human retinal vascular endothelial cells (HRVECs) were exposed to high glucose, oxidative stress, or inflammatory stimulus to mimic diabetic stress in vitro. Compared with the NG group, high glucose (30 mM) induced cZNF532 expression in pericytes after 24-hour or 48-hour treatment (Figure 1E). A similar result was observed in pericytes upon oxidative stress (H_2O_2, 100 μm) or inflammatory stimulus, such as VEGF (20 ng/mL), TNF-α (50 ng/mL), or IL-6 (50 ng/mL) (Figure 1F). By contrast, high glucose, oxidative stress, or inflammatory stimulus did not affect cZNF532 expression in HRVECs after 24-hour or 48-hour treatment (Figure 1, G and H).

To understand the mechanism of cZNF532 induction under diabetic conditions, we examined its transcriptional regulation. Analysis by the TRANSFAC database revealed the binding sites of several transcription factors in the sequence of cZNF532, including SP1, a transcription factor involved in the pathogenesis of diabetes (23). SP1 induction was observed in pericytes following high glucose or oxidative stress (Supplemental Figure 1D). SP1 silencing led to a marked reduction of cZNF532 expression (Supplemental Figure 1E). Normal pericytes and SP1 silencing pericytes were exposed to high glucose or oxidative stress for 12 hours. Chromatin immunoprecipitation assays were conducted to examine the binding between SP1 and the promoter region of cZNF532. DNA fragments were pulled down by a specific SP1 antibody. Upon high glucose or oxidative stress, more DNA fragments were pulled down by SP1 antibody in normal pericytes than in SP1 silencing pericytes (Supplemental Figure 1F).

cZNF532 regulates pericyte function in vitro. We determined whether cZNF532 regulated pericyte function in vitro. The expression of cZNF532 but not ZNF532 mRNA was significantly decreased after the transfection of cZNF532 siRNA (Supplemental Figure 2). Pericytes are multipotent stem and/or progenitor cells, which can be differentiated into many different cell types (3). cZNF532 silencing by cZNF532 siRNA1 reduced the expression of pericyte markers, including platelet-derived growth factor receptor β (PDGFR-β), α-SMA, Desmin, and NG2 (Figure 2A). Pericyte-endothelial cell crosstalk is important for vascular homeostasis. Pericyte recruitment is required for proper endothelial barrier function (2). Matrigel coculture assays revealed that cZNF532 silencing decreased pericyte recruitment toward HRVECs (Figure 2B). Pericytes were cocultured with HRVECs for 8 hours and 12 hours. Pericytes were seeded onto the basolateral side of the filter, while HRVECs were seeded onto the apical side. Aliquots were collected from the basolateral side 1, 2, 3, and 4 hours after the addition of FITC-dextran to the apical side. cZNF532 silencing in pericytes increased the permeability of macromolecules as compared with the control group (Figure 2C).

We then determined whether abnormal pericyte differentiation and recruitment was associated with altered cell viability or proliferation. MTT assays and Ki67 staining showed that cZNF532 silencing by cZNF532 siRNA1 decreased the viability and proliferation of pericytes (Figure 2, D and E). Flow cytometry analysis was conducted to determine cell cycle change. Compared with WT control group, cZNF532 silencing pericytes displayed a 3-fold reduction in S-phase cells and about a 30% increase in G1-phase cells (Figure 2F). We then determined whether cZNF532 silencing affected the development of pericyte apoptosis. PI staining and caspase-3/7 activity assays revealed that cZNF532 silencing by cZNF532 siRNA1 aggravated high glucose– or oxidative stress–induced cell apoptosis as shown by increased caspase-3/7 activity and increased PI^+ cells (Figure 2, G and H, and Supplemental Figure 3).

We also revealed that cZNF532 silencing by cZNF532 siRNA2 or siRNA3 reduced the expression of pericyte markers, decreased the recruitment of pericytes toward HRVECs, and decreased the viability and proliferation of pericytes (Supplemental Figure 4). Moreover, cZNF532 silencing by cZNF532 siRNA2 or siRNA3 aggravated high glucose– or oxidative stress–induced pericyte apoptosis (Supplemental Figure 5).

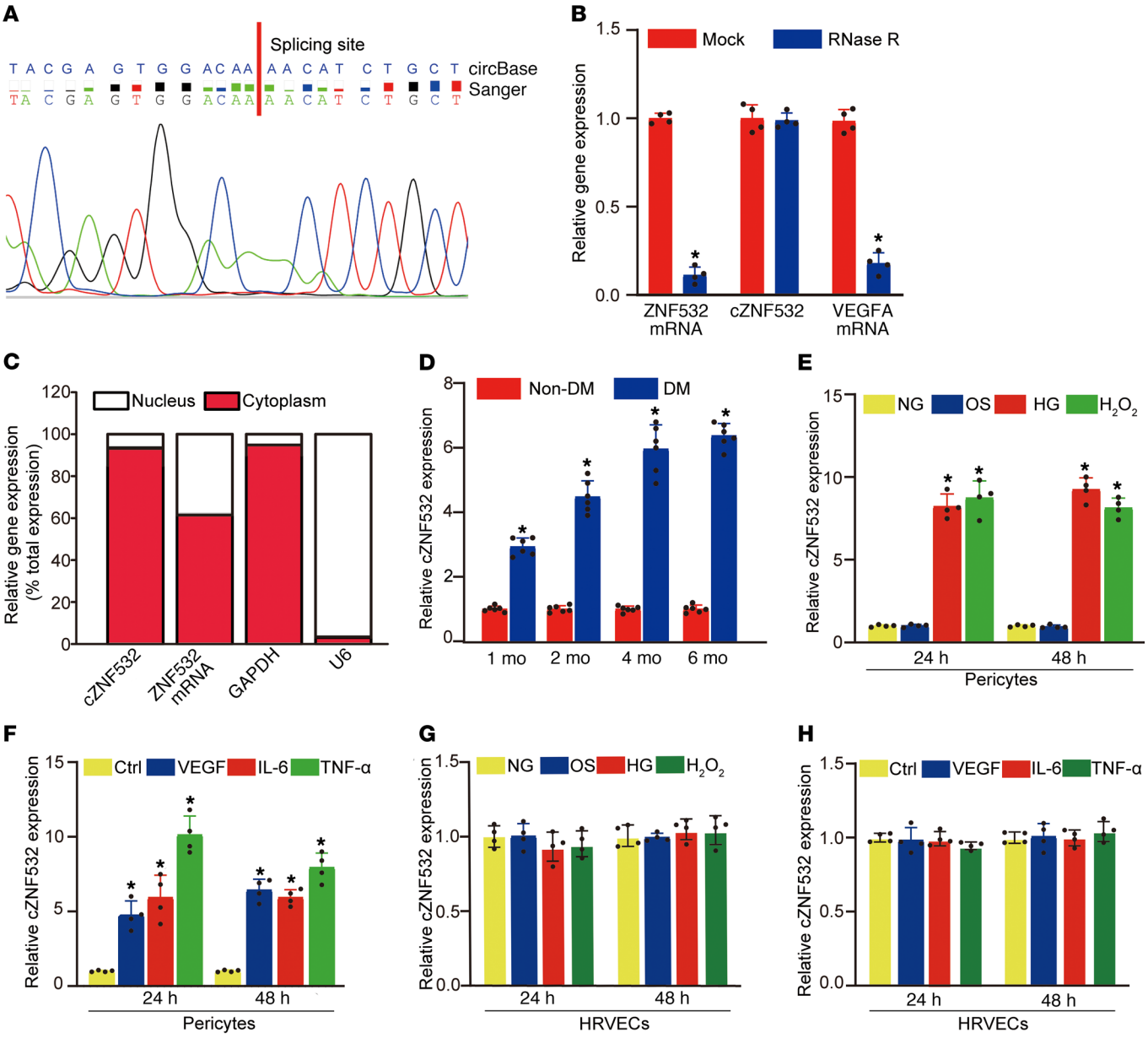

Figure 1. Identification of cZNF532 as a high glucose–regulated circRNA in pericytes. (**A**) Sanger sequencing was conducted to detect cZNF532 expression in pericytes. The result of Sanger sequencing (bottom) was consistent with the sequence of cZNF532 in circBase (top). (**B**) Total RNAs were digested with RNAse R followed by qRT-PCR detection of cZNF532 expression. ZNF532 mRNA and VEGFA mRNA was detected as the RNAse R–sensitive control ($n = 4$, Student's t test). (**C**) The expression of nucleus transcript (U6), cytoplasm transcript (GAPDH), ZNF532 mRNA, and cZNF532 was detected by qRT-PCRs in the nucleus and cytoplasm fraction of pericytes ($n = 4$). (**D**) cZNF532 expression was detected by qRT-PCRs in retinal vessels isolated from nondiabetic retinas and diabetic retinas 1 month, 2 months, 4 months, and 6 months after the induction of diabetes ($n = 6$ animals per group, Student's t test). The blood glucose levels of diabetic mice were above 300 mg/dL. (**E** and **G**) cZNF532 expression was detected by qRT-PCRs in pericytes (**E**) or HRVECs (**G**) cultured in medium containing normal glucose (NG, 5.55 mM), 5.55 mM glucose plus 24.45 mM pyruvate (osmotic control, OS), high glucose (HG, 30 mM), or H_2O_2 (100 μm) for 24 hours and 48 hours. (**F** and **H**) cZNF532 expression was detected by qRT-PCRs in pericytes (**F**) or HRVECs (**H**) cultured in the medium containing VEGF (20 ng/mL), IL-6 (50 ng/mL), and TNF-α (50 ng/mL) or left untreated (Ctrl) for 24 hours and 48 hours. For **E**–**H**, $^*P < 0.05$, 1-way ANOVA followed by Bonferroni's post hoc comparison test, error bar indicates SD.

We investigated whether cZNF532 silencing affected endothelial cell function in vitro. cZNF532 expression was downregulated after cZNF532 siRNA transfection in HRVECs (Supplemental Figure 6A). MTT and Ki67 staining assays showed that cZNF532 silencing did not affect the viability and proliferation of HRVECs (Supplemental Figure 6, B and C). PI staining and caspase-3/7 activity assays showed that cZNF532 silencing did not affect the development of high glucose– and oxidative stress–induced cell apoptosis (Supplemental Figure 6, D–G).

cZNF532 regulates retinal pericyte function and vascular integrity in vivo. Given the induction of cZNF532 in diabetic retinal vessels, we postulated that cZNF532 was involved in retinal

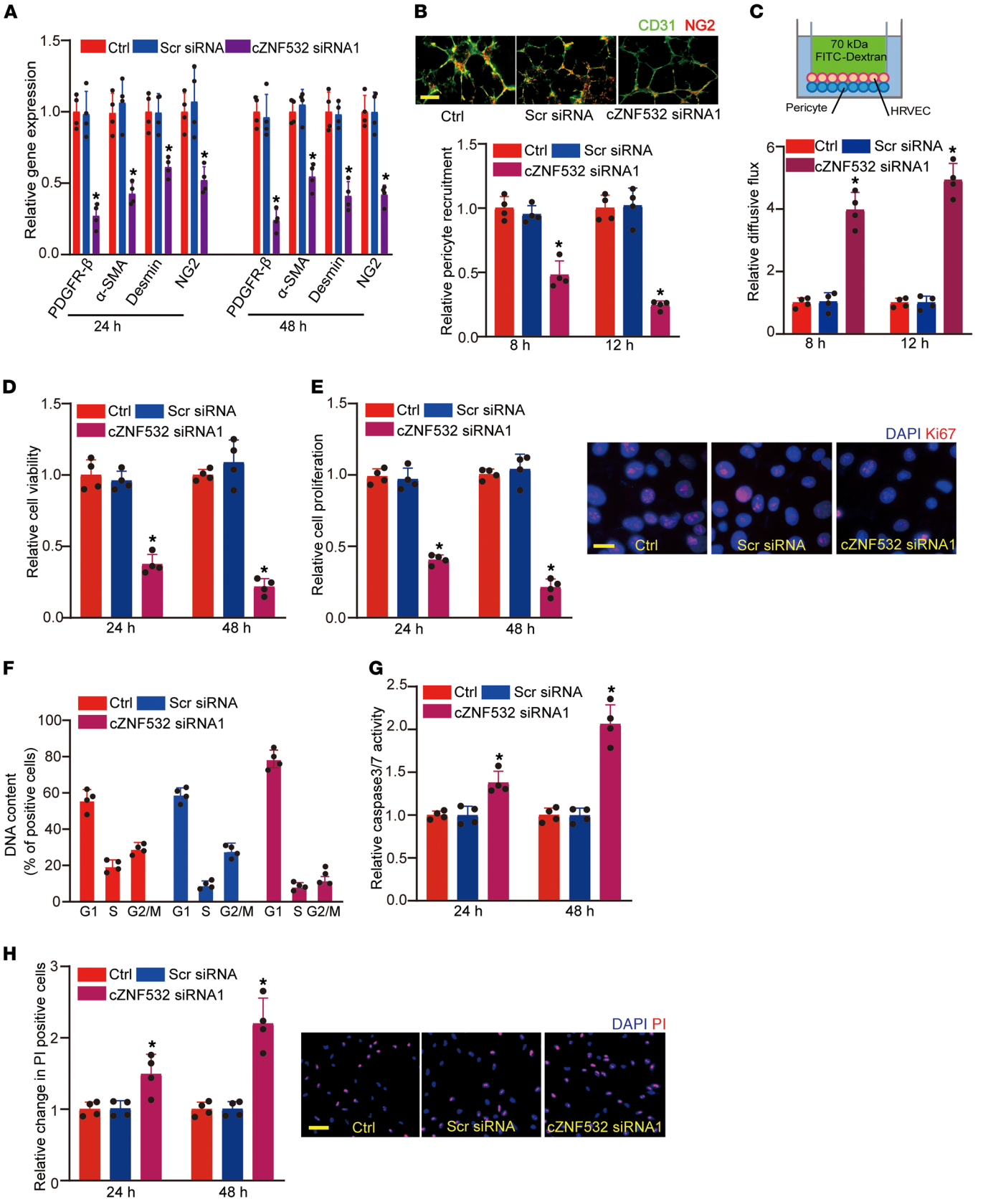
A
Ctrl
Scr siRNA
cZNF532 siRNA1
Relative gene expression
PDGFR-β
α-SMA
Desmin
NG2
24 h
48 h
B
CD31 NG2
Ctrl
Scr siRNA
cZNF532 siRNA1
Relative pericyte recruitment
8 h
12 h
C
70 kDa
FITC-Dextran
Pericyte
HRVEC
Relative diffusive flux
D
Relative cell viability
E
Relative cell proliferation
DAPI Ki67
F
DNA content
(% of positive cells)
G1
S
G2/M
G
Relative caspase3/7 activity
H
Relative change in PI positive cells
DAPI PI

Figure 2. cZNF532 regulates pericyte function in vitro. (**A**) The expression of pericyte markers, including PDGFR-β, α-SMA, desmin, and NG2, was detected by qRT-PCRs in pericytes after the transfection of scrambled (Scr) siRNA or cZNF532 siRNA1, or left untreated (Ctrl) for 24 hours and 48 hours (n = 4). (**B**) WT (Ctrl), cZNF532 siRNA1, or Scr siRNA–transfected pericytes were cocultured with HRVECs for 8 hours or 12 hours and then stained with NG2 (pericytes) and CD31 (HRVECs) to detect the recruitment of pericytes toward HRVECs (n = 4). The representative images at 12 hours are shown. Scale bar: 100 μm. (**C**) WT (Ctrl), cZNF532 siRNA1, or Scr siRNA–transfected pericytes were cocultured with HRVECs for 8 hours and 12 hours. Fluorescent solute (FITC-Dextran, 70 kDa) was added to the apical chamber and the rate of flux across the HRVEC monolayer was detected by a microplate reader. Endothelial barrier permeability was shown as relative diffusive flux change (n = 4). Average Po for the control samples at 8 hours and 12 hours was 2.78×10^{-6} cm/sec and 1.62×10^{-6} cm/sec, respectively. (**D** and **E**) Pericytes were transfected with Scr siRNA or cZNF532 siRNA1, or left untreated (Ctrl) for 24 hours or 48 hours. Cell viability was detected by MTT method (**D**, n = 4). Cell proliferation was detected by Ki67 staining. The representative images at 48 hours were shown (**E**, scale bar: 20 μm, n = 4). (**F**) Cell cycles of pericytes were detected by flow cytometry 48 hours after the transfection of Scr siRNA or cZNF532 siRNA1. Cell percentage in each phase was calculated by BD Cell Quest Pro software. (**G** and **H**) Pericytes were transfected with Scr siRNA or cZNF532 siRNA1, or left untreated (Ctrl), and then exposed to 30 mM glucose for 24 hours or 48 hours. Apoptotic cells were detected by caspase-3/7 activity (**G**, n = 4) or PI staining (**H**, n = 4). Representative PI staining images at 48 hours were shown (scale bar: 100 μm). All significant difference was determined by 1-way ANOVA followed by Bonferroni's post hoc test. Error bar indicates SD. $^*P < 0.05$.

vascular dysfunction. Intravitreous injection of cZNF532 shRNA reduced the expression of cZNF532 but not ZNF532 mRNA (Supplemental Figure 7, A and B). We used cZNF532 shRNA1 for subsequent experiments because it had the greatest silencing efficiency. Injection of cZNF532 shRNA1 significantly reduced retinal cZNF532 expression but not ZNF532 mRNA expression throughout the experiment (Supplemental Figure 7, C and D). STZ injection induced hyperglycemia and a phenotype strongly resembling type 1 diabetes mellitus and diabetic retinopathy. We used an STZ-induced diabetic model to investigate the role of cZNF532 in retinal vascular dysfunction. cZNF532 shRNA1 injection did not further change the glycemic level and body weight of diabetic mice (diabetic+cZNF532 shRNA) as compared with diabetic group (diabetic+Scr shRNA) (Supplemental Table 1). cZNF532 shRNA1 injection did not induce a detectable immune response as shown by unchanged expression of IL-6 and MCP-1 in the serum and vitreous compared with PBS-injected control (Supplemental Figure 7, E and F).

IB4 and NG2 immunofluorescence staining was conducted to detect pericyte coverage of retinal vessels. At 1 month, cZNF532 silencing alone (cZNF532 shRNA) or DR alone did not affect pericyte coverage. The combination of cZNF532 silencing and diabetes (DR + cZNF532 shRNA) reduced pericyte coverage. cZNF532 shRNA alone or DR alone reduced retinal pericyte coverage at 2 months, 4 months, and 6 months. Combine of cZNF532 silencing and diabetes further reduced retinal pericyte coverage (Figure 3, A and B). These results show that the experimental factors, cZNF532 silencing and diabetes, regulated pericyte coverage in a synergistic manner. Evans blue (EB) assays were conducted to detect retinal vascular leakage. We also revealed that the experimental factors, cZNF532 silencing and diabetes, aggravated diabetes-induced retinal vascular leakage in a synergistic manner at 1 month, 2 months, 4 months, and 6 months, which was similar to the result of cZNF532-regulated pericyte coverage (Figure 3, C and D). Acellular vascular, microaneurysm, and pericyte loss are the typical pathological features of diabetic retinas (24). Trypsin digest and periodic acid Schiff (PAS) staining was conducted to detect the structural change of retinal vessels. Nondiabetic retinas injected with cZNF532 shRNA generated diabetic vascular pathology as shown by the appearance of retinal microaneurysms, acellular capillaries, and pericyte ghosts after 2 months, 4 months, and 6 months of treatment. In diabetic retinas, cZNF532 silencing further increased the number of microaneurysms, acellular capillaries, and pericyte ghosts (Supplemental Figure 8, A–D). DR is usually associated with inflammatory response due to vascular impairment (9). ELISAs revealed that cZNF532 silencing aggravated diabetes-induced retinal inflammatory response after 6 months of treatment as shown by increased expression of IL-2, IL-6, TNF-α, VEGF, and MCP-1 (Supplemental Figure 8E).

We further asked whether cZNF532 overexpression alleviated diabetes-induced retinal vascular dysfunction. cZNF532 overexpression protected against retinal vascular dysfunction as shown by increased pericyte coverage, decreased vascular permeability as shown by reduced EB extravasation, and decreased number of microaneurysms, acellular capillaries, and pericyte ghosts (Supplemental Figure 9). Collectively, the above-mentioned results indicate that cZNF532 regulates retinal pericyte function and vascular integrity in vivo.

Conditional knockdown of cZNF532 in pericytes induces retinal vascular dysfunction in vivo. The above-mentioned results reveal that nonspecific knockdown of cZNF532 induced retinal vascular function. The retina is composed of tremendously diverse cell types. However, it is still challenging to knockout a gene especially a circRNA in a specific cell type (25). Since hundreds of gene-specific promoter–driven Cre mouse lines are available, cZNF532 shRNA was subcloned into the Cre-dependent AAV vector, pAKD-CMV-bGlobin-EGFP-cZNF532 shRNA. Intravitreous injection of Cre-dependent cZNF532 shRNA in PDGFR-β-cre mice decreased cZNF532 expression in pericytes but not in endothelial cells (Supplemental Figure 10).

IB4 and NG2 staining showed that compared with nondiabetic Cre group (Cre) or diabetic Cre group (Cre-DR), pericyte-specific cZNF532 knockdown (DR + cZNF532 shRNA) reduced pericyte coverage of retinal vessels at 1 month, 2 months, 4 months, and 6 months after the administration of Cre-dependent cZNF532 shRNA (Figure 4, A and B). EB assays showed that compared with Cre group or DR group, pericyte-specific cZNF532 knockdown (DR + cZNF532 shRNA) further aggravated retinal vascular leakage (Figure 4, C and D). Trypsin digest and PAS staining showed that nondiabetic Cre retinas (Cre) injected with Cre-dependent cZNF532 shRNA generated diabetic vascular pathology as shown by the appearance of retinal microaneurysms, acellular capillaries, and pericyte ghosts. Compared with diabetic Cre group (Cre-DR), cZNF532 silencing in pericytes (DR + cZNF532 shRNA) further increased the number of microaneurysms, acellular capillaries, and pericyte ghosts (Supplemental Figure 11, A–C). ELISAs revealed that pericyte-specific cZNF532 knockdown aggravated

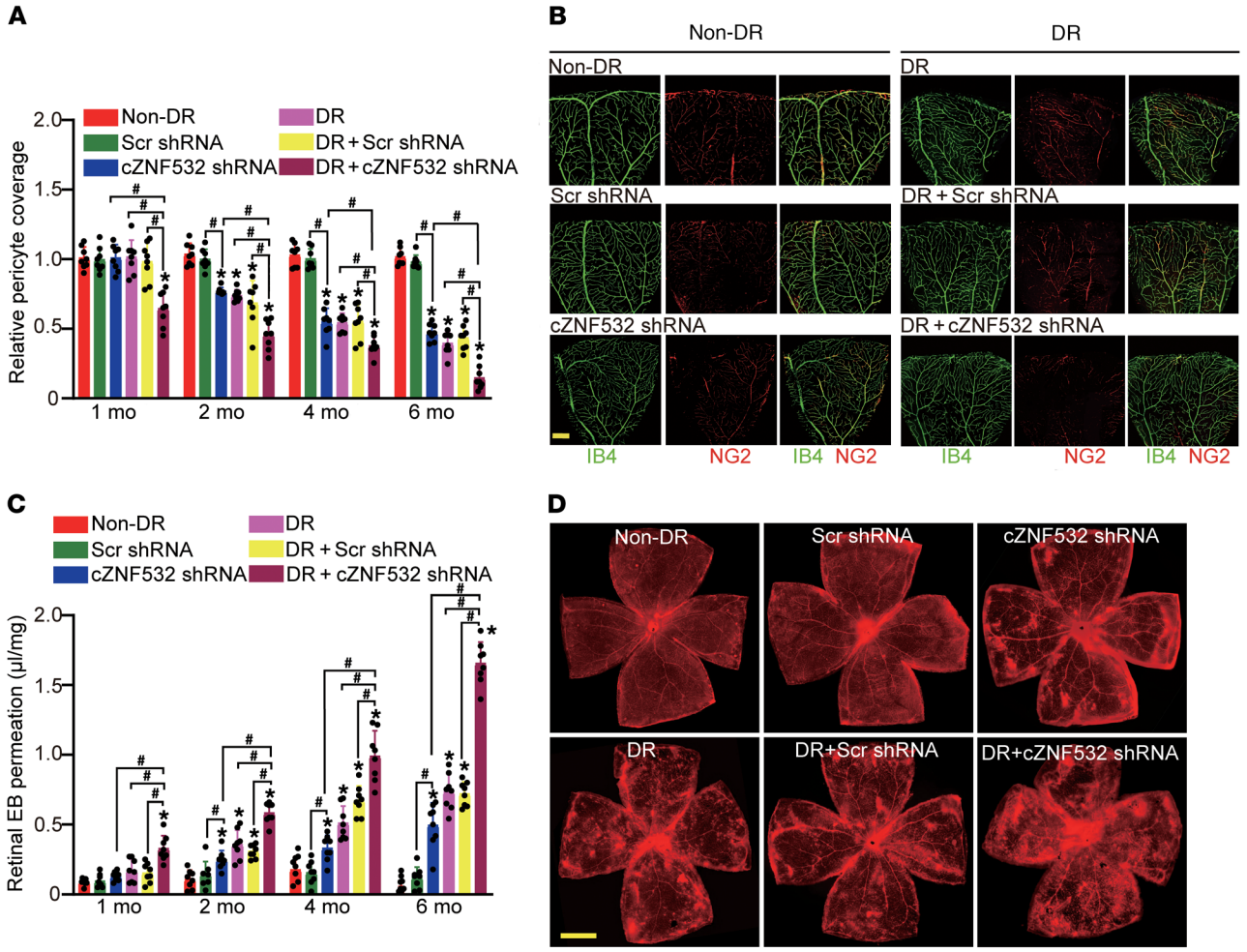

Figure 3. cZNF532 regulates retinal pericyte function and vascular integrity in vivo. (**A** and **B**) Pericyte coverage was quantified by staining the whole-mount retina with Isolectin IB4 and NG2 in the nondiabetic C57BL/6 mice (non-DR) or diabetic mice (Cre-DR) without or with intravitreous injection of Scr shRNA or cZNF532 shRNA after 1 month, 2 months, 4 months, or 6 months of treatment. To visualize a whole leaf of retinal vessel, tile scanning was used whereby multiple overlapping (10%–20% overlap) images were captured by a ×10 lens with identical gain setting. The composite images were generated by arraying the individual images in Adobe Photoshop. The statistical result (**A**, $n = 8$) and representative composite images after 6 months of treatment are shown (**B**, scale bar: 100 μm). (**C** and **D**) The mice were infused with Evans blue (EB) dye for 2 hours. The tile-scanning images of whole retinal vessels were taken using a ×4 lens with identical gain settings. The statistical result of EB extravasation (**C**, $n = 8$) and representative images of flat-mounted retinas after 6 months of treatment (**D**, scale bar: 500 μm). The red fluorescence indicates EB signal. The blood glucose levels of diabetic mice were above 300 mg/dL. All significant differences were evaluated by Mann-Whitney *U* test or Kruskal-Wallis's test followed by Bonferroni's post hoc test. Error bar indicates SD. $^{*}P < 0.05$ compared with non-DR group; $^{\#}P < 0.05$ between the marked groups.

retinal inflammatory response as shown by increased expression of IL-2, IL-6, TNF-α, VEGF, and MCP-1 (Supplemental Figure 11D).

cZNF532 regulates pericyte function by acting as a sponge for miR-29a-3p in vitro. Since cZNF532 was mainly expressed in the cytoplasm of pericytes, we speculated that cZNF532 regulated pericyte function at the posttranscriptional level by acting as miRNA sponge. We searched for cZNF532-interacting miRNAs by the TargetScan algorithm, which can predict miRNAs that target circRNAs by surveying for 7-mer or 8-mer complementarity to the seed region (Supplemental Table 2). The entire cZNF532 sequence was inserted into pGL3 luciferase reporter to generate LUC-cZNF532 vector. Luciferase activity screening showed that miR-29a-3p, miR-498, and miR-758 mimic transfection decreased the luciferase activity of LUC-cZNF532 (Figure 5A). By contrast, miR-29a-3p, miR-498, or miR-758 mimic transfection did not change the luciferase activity of LUC-cZNF532 mutant, which did not have the binding sites of these miRNAs (Figure 5B). We determined the relative expression abundance of cZNF532, miR-29a-3p, miR-498, and miR-758 in pericytes and mouse retinas. miR-29a-3p had similar expression abundance as cZNF532 and higher expression abundance than miR-498 and miR-758 (Figure 5, C and D). Due to the high abundance, we mainly investigated the role of miR-29a-3p in pericytes. If cZNF532 had the potency as a sponge for miR-29a-3p, it should coexpress with miR-29a-3p and have a limited number of miR-29a-3p target sites. FISH assay revealed the overlapping coexpression of cZNF532 and miR-29a-3p in the cytoplasm of pericytes (Figure 5E). cZNF532 had 3 potential miR-29a-3p binding sites (Figure 5F).

We further employed a luciferase activity assay to investigate whether cZNF532 could bind to miR-29a-3p. The perfect target

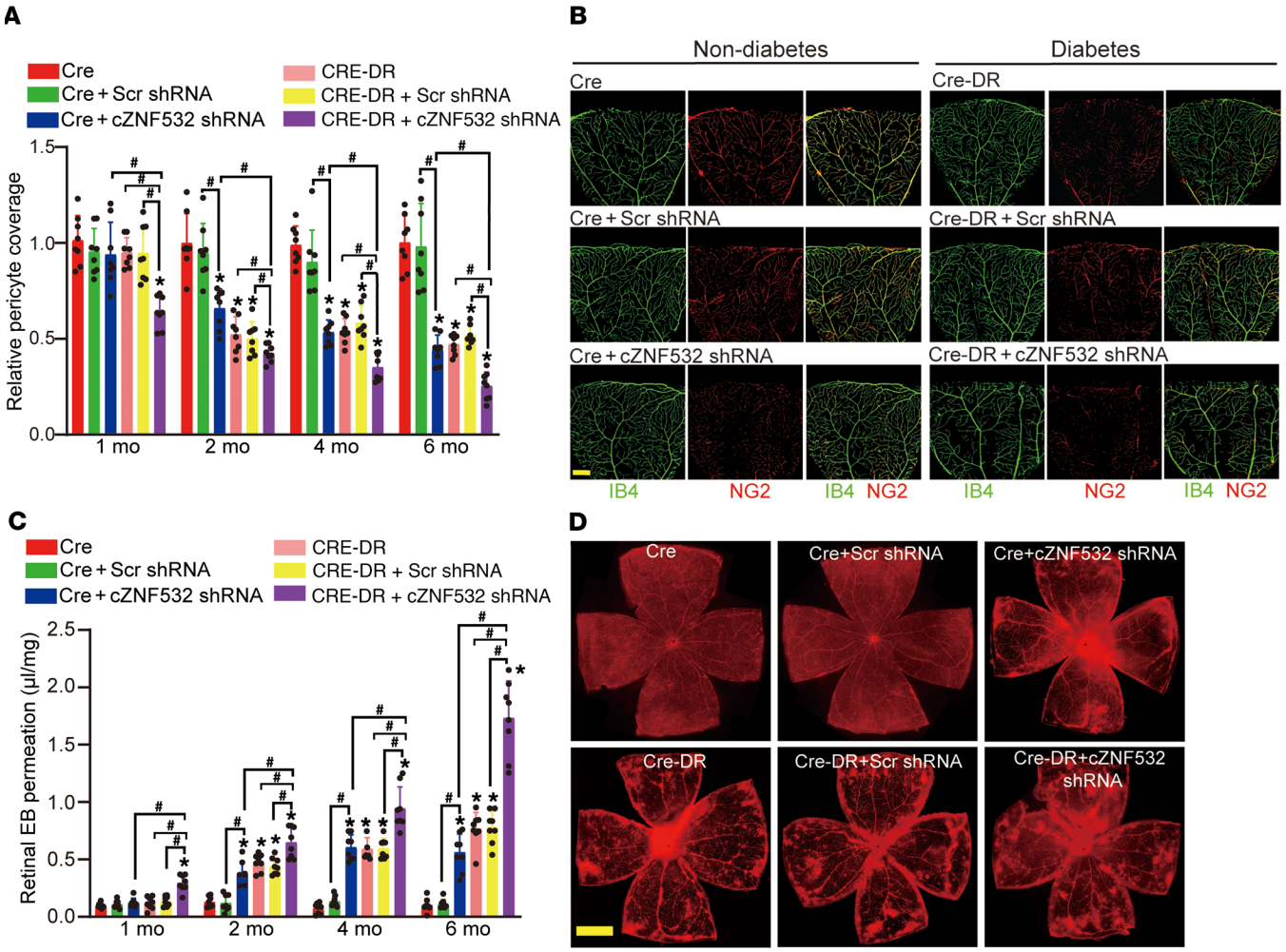

Figure 4. Conditional knockdown of cZNF532 in pericytes induces retinal vascular dysfunction in vivo. (**A** and **B**) Pericyte coverage was quantified by staining the whole-mount retinas with Isolectin IB4 and NG2 in nondiabetic C57BL/6 Cre mice (Cre) or diabetic Cre mice (Cre-DR) without or with intravitreous injection of Scr shRNA or cZNF532 shRNA after 1, 2, 4, or 6 months of treatment (n = 8; scale bar: 100 μm). Tile scanning and Adobe Photoshop were used to generate the composite images of a whole leaf of retinal vessels. The statistical result and representative images after 6 months of treatment are shown. (**C** and **D**) The mice were infused with EB dye for 2 hours. The tile-scanning images of whole retinal vessels were taken using a ×4 lens with identical gain settings. The statistical result of EB extravasation and representative images of flat-mounted retinas after 6 months of treatment (n = 8; scale bar, 500 μm). The red fluorescence indicates EB signal. The blood glucose levels of diabetic mice were above 300 mg/dL. All significant differences were evaluated by Mann-Whitney U test or Kruskal-Wallis test followed by Bonferroni's post hoc test. Error bar indicates SD. $^{*}P < 0.05$ compared with Cre group. $^{\#}P < 0.05$ among the marked groups.

sequence of miR-29a-3p or the entire cZNF532 sequence was inserted into the pGL3 vector to generate 2 luciferase reporters. miR-29a-3p could bind to the above-mentioned reporters and decrease the luciferase activity. cZNF532 overexpression or anti–miR-29a-3p reversed miR-29a-3p–mediated repression of luciferase activity. By contrast, cZNF532-ir vector, which could not produce cZNF532, had a minor effect due to low cZNF532 production or inefficient circularization (Figure 5, G and H). We also revealed that transfection of miR-29a-3p inhibitor or mimic did not change the expression of cZNF532 and ZNF532 mRNA in pericytes (Figure 5I). These results suggest that cZNF532 only acted as a sponge for miR-29a-3p and impaired miR-29a-3p activity through sequestering miR-29a-3p from its target genes.

We employed TargetScan to predict the target genes of miR-29a-3p. Three candidate genes, including CSPG4 (NG2), lysyl oxidase like 2 (LOXL2), and cyclin-dependent kinase 2 (CDK2), aroused our interests due to their roles in cell differentiation, migration, and proliferation (26–28). miR-29a-3p mimic transfection downregulated CSPG4, LOXL2, and CDK2 expression (Supplemental Figure 12A). The 3′-UTR of CSPG4, LOXL2, or CDK2 genes was cloned into the luciferase vector and cotransfected with miR-29a-3p mimic into HEK293T cells. A significant reduction in luciferase activity was detected in the presence of miR-29a-3p mimic, whereas the mutation of miR-29a-3p target site completely abolished the repression (Supplemental Figure 12B). cZNF532 silencing also reduced the expression of CSPG4, LOXL2, and CDK2 (Supplemental Figure 12C).

We also investigated the role of miR-29a-3p in pericytes. miR-29a-3p mimic transfection reduced the expression of pericyte markers, including PDGFR-β, α-SMA, desmin, and NG2 (Sup-

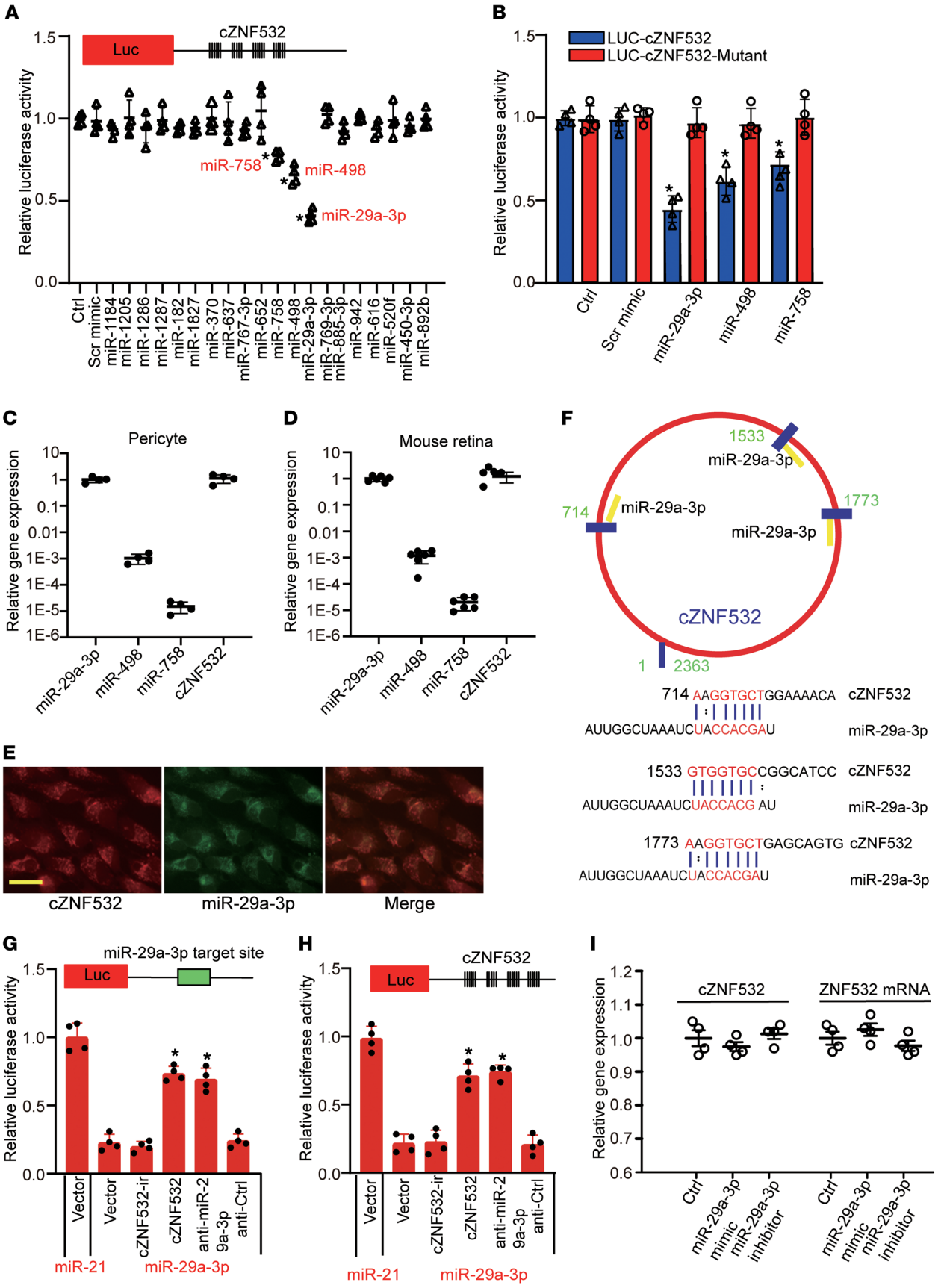
A
Luc
cZNF532
Relative luciferase activity
miR-758
miR-498
miR-29a-3p
Ctrl
Scr mimic
miR-1184
miR-1205
miR-1286
miR-1287
miR-182
miR-1827
miR-370
miR-637
miR-767-3p
miR-652
miR-758
miR-498
miR-29a-3p
miR-769-3p
miR-885-3p
miR-942
miR-616
miR-520f
miR-450-3p
miR-892b
B
LUC-cZNF532
LUC-cZNF532-Mutant
Relative luciferase activity
Ctrl
Scr mimic
miR-29a-3p
miR-498
miR-758
C
Pericyte
Relative gene expression
miR-29a-3p
miR-498
miR-758
cZNF532
D
Mouse retina
Relative gene expression
miR-29a-3p
miR-498
miR-758
cZNF532
E
cZNF532
miR-29a-3p
Merge
F
1533
miR-29a-3p
714
miR-29a-3p
1773
miR-29a-3p
cZNF532
1
2363
714 AAGGTGCTGGAAAACA cZNF532
AUUGGCUAAAUCUACCACGAU miR-29a-3p
1533 GTGGTGCCGGCATCC cZNF532
AUUGGCUAAAUCUACCACG AU miR-29a-3p
1773 AAGGTGCTGAGCAGTG cZNF532
AUUGGCUAAAUCUACCACGAU miR-29a-3p
G
miR-29a-3p target site
Luc
Relative luciferase activity
Vector
Vector
cZNF532-ir
cZNF532
anti-miR-29a-3p
anti-Ctrl
miR-21
miR-29a-3p
H
cZNF532
Luc
Relative luciferase activity
Vector
Vector
cZNF532-ir
cZNF532
anti-miR-29a-3p
anti-Ctrl
miR-21
miR-29a-3p
I
cZNF532
ZNF532 mRNA
Relative gene expression
Ctrl
miR-29a-3p mimic
miR-29a-3p inhibitor
Ctrl
miR-29a-3p mimic
miR-29a-3p inhibitor

Figure 5. cZNF532 regulates pericyte function by acting as a miRNA sponge in vitro. (**A**) HEK293T cells were transfected with pGL3-Basic (Ctrl) or LUC-cZNF532 with different miRNA mimic and pRL-TK vector. pRL-TK vector was transfected as the internal transfection control. Luciferase assays were conducted 48 hours after transfection using the Dual-Luciferase Reporter Assay kit. Normalized value of luciferase activity for Ctrl group was set to 1 (n = 4). (**B**) LUC-cZNF532 or LUC-cZNF532-mutant was cotransfected without or with miRNA mimic and pRL-TK vector. Luciferase assays were conducted 48 hours after transfection. Normalized value of luciferase activity was set to 1 in cells transfected with LUC-cZNF532 and pRL-TK (n = 4). (**C** and **D**) Relative expression abundance of cZNF532, miR-29a-3p, miR-498, and miR-758 was detected by qRT-PCR in pericytes (**C**, n = 4) and mouse retinas (**D**, n = 6). (**E**) Expression distribution of cZNF532 and miR-29a-3p in pericytes was detected by RNA-FISH assay (scale bar: 20 μm). (**F**) The schematic figure shows the putative binding sites of miR-29a-3p on cZNF532 transcript. (**G** and **H**) Luciferase reporter with perfect miR-29a-3p target site (**G**) or entire cZNF532 sequence was constructed (**H**). The constructed reporter was transfected with 40 ng empty vector (vector, pcDNA3), 40 ng cZNF532-ir (pcDNA3-cZNF532-ir), 40 ng cZNF532 (pcDNA3-cZNF532), 5 nM anti–miR-29a-3p (anti–miR-29a-3p), or 5 nM anti–miRNA control (anti-Ctl), together with 20 ng pJEBB-miR-29a-3p or pJEBB-miR-21 expression plasmid. Meanwhile, pRL-TK vector was transfected as the internal control. The normalized value of luciferase activity was set to 1 in cells transfected with the constructed Luc reporter, pcDNA3 (vector), pJEBB-miR-21, and pRL-TK. Luciferase activity was detected at 48 hours after transfection (n = 4, $^*P < 0.05$ vs. miR-29a-3p plus vector). (**I**) Pericytes were transfected with miR-29a-3p mimic or miR-29a-3p inhibitor, or left untreated (Ctrl) for 48 hours. The expression of cZNF532 and ZNF532 mRNA was detected by qRT-PCR (n = 4). The significant difference was determined by 1-way ANOVA followed by Bonferroni's post hoc test. Error bar indicates SD. $^*P < 0.05$.

plemental Figure 12D), decreased the recruitment of pericytes toward HRVECs (Supplemental Figure 12E), and decreased the viability and proliferation of pericytes (Supplemental Figure 12, F and G). cZNF532 overexpression reversed miR-29a-3p–mediated effects on pericyte function. PI staining and caspase-3/7 activity assays revealed that miR-29a-3p mimic transfection aggravated high glucose– or oxidative stress–induced cell apoptosis as shown by increased PI^+ cells and caspase-3/7 activity. cZNF532 overexpression partially alleviated miR-29a-3p–mediated proapoptotic effects on pericytes (Supplemental Figure 13).

cZNF532-miR-29a-3p-NG2/LOXL2/CDK2 network regulates pericyte function and vascular integrity in vivo. We then investigated the role of miR-29a-3p in retinal vascular dysfunction in vivo. miR-29a-3p agomir or cZNF532 silencing led to increased expression of NG2, LOXL2, and CDK2 (Supplemental Figure 14). miR-29a-3p agomir could mimic the effects of cZNF532 silencing on retinal vascular dysfunction. In diabetic retina, injection of miR-29a-3p agomir decreased pericyte coverage (Figure 6, A and B), aggravated vascular leakage (Figure 6, C and D), and increased the number of microaneurysms, acellular capillaries, and pericyte ghosts (Figure 6, E–G).

We then determined whether exogenous intervention of miR-29a-3p overwhelmed the sponge function of cZNF532. cZNF532 silencing released the sponged miR-29a-3p. Compared with the DR group (Ctrl), miR-29a-3p inhibition by miR-29a-3p antagomir reversed cZNF532 silencing–induced pericyte degeneration (Supplemental Figure 15, A and B), reduced cZNF532 silencing–induced retinal vascular leakage (Supplemental Figure 15C), and decreased the number of microaneurysms, acellular capillaries, and pericyte ghosts (Supplemental Figure 15, D–F) at 2 months, 4 months, and 6 months after treatment.

Clinical implication of cZNF532/miR-29a-3p/NG2, LOXL2, and CDK2 signaling in retinal vascular dysfunction. We subsequently investigated the clinical implication of dysregulated cZNF532/miR-29a-3p/NG2, LOXL2, and CDK2 signaling. We collected the vitreous samples during vitrectomy from 36 subjects. These samples were divided into 4 categories based on disease severity: nondiabetic control samples (Ctrl, n = 8 eyes), diabetic macular edema (DME) without proliferative diabetic retinopathy (PDR) (n = 12 eyes), DME with PDR (n = 12 eyes), and neovascularization of the iris (NVI), representing the most fulminate version of DR (n = 4 eyes) (Supplemental Table 3). qRT-PCRs showed that cZNF532 expression was upregulated in the vitreous of patients with DME, PDR, or NVI and its expression was correlated with disease severity (Figure 7A). By contrast, miR-29a-3p expression was not altered in the vitreous of patients among the 4 categories (Figure 7B). ELISAs showed that NG2, LOXL2, or CDK2 concentration was upregulated in the vitreous of patients with DME, PDR, or NVI compared with nondiabetic control samples (Supplemental Table 4). Pericytes were incubated with the vitreous from PDR patients. Caspase-3/7 activity assay or PI staining assays revealed that induction of cZNF532-mediated signaling by overexpression of cZNF532 or inhibition of miR-29a-3p protected pericytes against diabetic vitreous–induced pericyte apoptosis (Figure 7, C and D). Animal studies have revealed that cZNF532 overexpression protected against diabetes-induced retinal vascular dysfunction. cZNF532 was upregulated in the clinical samples of the patients with DR. We postulated that cZNF532 acted as a protector in the etiology of diabetic retinopathy. EB assays revealed that intravitreous injection of human diabetic vitreous led to increased retinal vasopermeability, which was similar to previous studies (29, 30). Coinjection of cZNF532 overexpression vector or miR-29a-3p antagomir reduced diabetic vitreous–induced effect on retinal vasopermeability, which was similar to the effect of anti-VEGF on retinal vasopermeability (Figure 7E). NG2 and IB4 staining showed that cZNF532 overexpression or miR-29a-3p inhibition decreased diabetic vitreous–induced pericyte degeneration (Figure 7F).

Discussion

A mechanistic understanding of DR pathogenesis has evolved in recent years to encompass pericyte degeneration in addition to endothelial dysfunction. This view is particularly plausible due to the pivotal role of pericytes in vascular maturation, homeostasis, and remodeling (26). In this study, we show that cZNF532 expression is upregulated in pericytes under diabetic stress, in the retinal vessels of a diabetic murine model, and in the vitreous humor of diabetic patients. cZNF532 regulates retinal pericyte degeneration and vascular dysfunction by acting as a miR-29a-3p sponge and inducing increased expression of NG2, LOXL2, and CDK2 (Figure 8). cZNF532 overexpression or miR-29a-3p inhibition protects against diabetes-induced retinal pericyte degeneration and vascular dysfunction.

Hyperglycemia and oxidative stress are the major pathological factors in DR (31, 32). They induce the expression of SP1 transcription factor. The involvement of SP1 in the pathogenesis

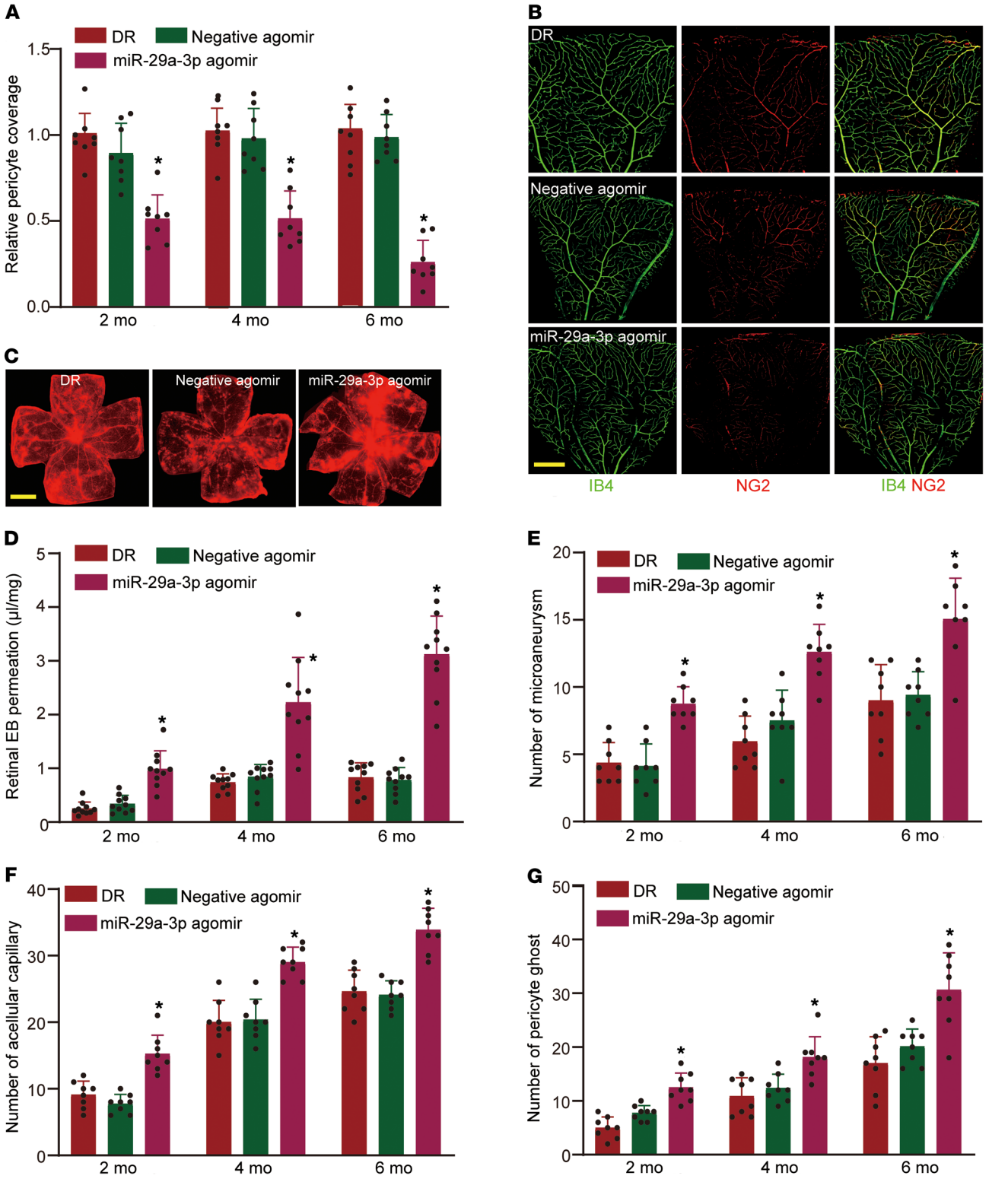

Figure 6. cZNF532-miR-29a-3p-NG2/LOXL2/CDK2 signaling regulates retinal pericyte function and vascular integrity in vivo. (**A** and **B**) Diabetic C57BL/6 mice (3 months old, male) received an intravitreous injection of miR-29a-3p agomir or negative control (NC) agomir, or were left untreated (Ctrl). Pericyte coverage was quantified by staining the whole-mount retinas with Isolectin IB4 and NG2 after 2 months, 4 months, and 6 months of treatment (n = 8; scale bar: 100 μm). The statistical result and representative images after 6 months of treatment are shown. (**C** and **D**) The above-mentioned mice were infused with EB dye for 2 hours. The tile-scanning images of entire retinal vessels were taken using a ×4 lens with identical gain settings. The representative images of flat-mounted retinas after 6 months of treatment (**C**, n = 10; scale bar: 500 μm) and statistical result of EB extravasation are shown (**D**). The red fluorescence indicates EB signal. (**E**–**G**) Retinal trypsin digestion and PAS staining were conducted to detect the number of microaneurysms (**E**, n = 8 per mm^2 retina), acellular capillaries (**F**, n = 8 per mm^2 retina), and pericyte ghosts (**G**, n = 8 per mm^2 retina). The blood glucose levels of diabetic mice were above 300 mg/dL. The significant difference was evaluated by Kruskal-Wallis's test followed by Bonferroni's post hoc test. Error bar indicates SD. *P < 0.05.

of diabetes has been recognized previously (33, 34). SP1 binds to the promoter region of cZNF532 and activates cZNF532 transcription. Vision loss in DR is primarily ascribed to retinal vascular dysfunction, including pericyte degeneration, hyperpermeability, hypoperfusion, and angiogenesis, which eventually cause retinal anatomical and functional changes (35). Pericyte degeneration is the earliest event during retinal vascular dysfunction. cZNF532 silencing decreases pericyte coverage in retinal capillaries. Pericyte loss from retinal capillaries can induce the breakdown of the blood-retinal barrier (BRB) followed by hyperpermeability and the inflammatory response (35). cZNF532 silencing aggravates diabetes-induced retinal vascular leakage and inflammation. Hyperglycemia also induces the progressive loss of retinal capillary cells and the generation of acellular capillaries and microaneurysms (36). cZNF532 silencing increases the number of nonperfused acellular capillaries and microaneurysms. By contrast, cZNF532 overexpression protects against diabetes-induced retinal vascular dysfunction. Thus, cZNF532 induction is critical for maintaining pericyte function and vascular homeostasis. cZNF532 induction is a compensatory response to diabetic stress. cZNF532 induction increases the proliferation and recruitment of pericytes, protects pericytes against diabetic stress, and retards the progression of retinal vascular dysfunction.

Pericyte degeneration is the primary clinical manifestation in the diabetic retina (32). Our results show that cZNF532 expression is deregulated in pericytes but not in endothelial cells. Activation of cZNF532-mediated signaling appears to protect against diabetes-induced pericyte degeneration. However, it is still challenging to knock out a gene, especially a circRNA in a specific retinal cell. Since hundreds of gene-specific promoter–driven Cre mouse lines are available (25, 37), we designed Cre-dependent expression of cZNF532 shRNA and injected this shRNA into the vitreous of PDGFR-β-Cre mouse eyes. Cre-dependent expression of cZNF532 shRNA silences cZNF532 expression in pericytes. Moreover, conditional knockdown of cZNF532 in pericytes induces pericyte degeneration and aggravates retinal vascular dysfunction. The evidence suggests that cZNF532 protects against retinal vascular dysfunction mainly through governing pericyte biology.

circRNAs usually play their roles by acting as the sponges for miRNAs or proteins, competing with the linear mRNA, or regulating the transcription of their parental genes (19). cZNF532 is mainly expressed in the cytoplasm of pericytes, suggesting a regulatory role at the posttranscriptional level. cZNF532 serves as a sponge for miR-29a-3p. NG2, LOXL2, and CDK2 are verified as the target genes of miR-29a-3p. NG2/CSPG4 is a cell-surface chondroitin sulphate proteoglycan that is expressed by numerous tissue-specific progenitor cells during development. It is turned off upon terminal differentiation, but it is reactivated in a diseased condition (38). NG2/CSPG4 participates in the regulation of pericyte function and basement membrane stability (39). LOXL2 mediates collagen stabilization and deposition in the extracellular matrix, suggesting a potential role in cell migration (40). CDK2 is a serine/threonine protein kinase that participates in cell-cycle regulation, and its expression is tightly associated with cell proliferation (41). Based on the above-mentioned evidence, we know that NG2/CSPG4, LOXL2, and CDK2 participate in cell differentiation, proliferation, and migration. Pericyte degeneration is associated with aberrant differentiation, proliferation, and migration. cZNF532 overexpression becomes a sink for miR-29-3p, and it releases the repressive effect of miR-29a-3p on NG2/CSPG4, LOXL2, and CDK2. Thus, it is not surprising that cZNF532-miR-29a-3p-NG2/LOXL2/CDK2 signaling is involved in pericyte degeneration.

Our results show that cZNF532 is upregulated in the vitreous of patients with DME, PDR, or NVI and its expression is correlated with the severity of DR. cZNF532 is shown as a promising biomarker for the diagnosis and prognosis of DR. cZNF532 overexpression or inhibition of its downstream molecule, miR-29a-3p, counteracts the effect of human diabetic vitreous–induced increased retinal vasopermeability and decreased pericyte coverage. The role of VEGF in vasopermeability and pericyte function has been recognized gradually. Delivery of anti-VEGF is a major treatment for diabetic eye diseases (42); however, a small number of the patients have no clinical response or a delayed response to anti-VEGF treatment (43). The composition of vitreous proteome changes with diabetes and molecular interactions with other molecules may potentiate endogenous VEGF effects even at a quite low concentration (28, 44). Since the eye is a small and self-contained compartment, high-level and region-restricted induction of cZNF532-mediated signaling may reduce endogenous VEGF effects and provide an alternative option for the treatment of retinal vascular dysfunction.

In conclusion, this study provides an attractive target (i.e., cZNF532) for the treatment of pericyte degeneration and retinal vascular dysfunction. However, our study has certain limitations. First, the retina is comprised of several cell types, including ganglion cells, cone photoreceptors, amacrine cells, horizontal cells, bipolar neurons, glial cells, and vascular cells (37). There are still obvious technical difficulties in performing conditional overexpression or knockdown of a circRNA in a specific cell type in the retina. Nonspecific knockdown or overexpression not only affects cZNF532 expression in pericytes but also in other retinal cells. Conditional knockdown by Cre-dependent cZNF532 shRNAs cannot completely remove cZNF532 expression in pericytes. The possible off-target effects are required to be examined to avoid the overestimation of cZNF532 function resulting from nonspecific intervention or incomplete inhibition of cZNF532. Second, retinal capillaries are mainly composed of endothelial cells and pericytes. In vitro studies have identified the cell-specific role of cZNF532 in pericytes. However, in vitro cultures may change the biological activities of endothelial cells and pericytes. It cannot completely reflect the dynamic and complicated cell-cell interactions in vivo. We thus cannot rule out the possibility that cZNF532 also regulates retinal vascular function through targeting endothelial cells in vivo. Even though the result that cZNF532 regulates retinal pericyte degeneration and vascular dysfunction is encouraging, we acknowledge that further studies are still required to define the precise role of cZNF532 in DR through the improvement of a conditional circRNA knockout technique.

Methods

Cell culture and transfection. Human retinal pericytes (ACBRI-183) and HRVECs (ACBRI-181) were obtained from Cell Systems Corporation (CSC). Human retinal pericytes (passages 4–7) were cultured in Dulbecco's modified Eagle's medium (DMEM, Gibco) at 5.5 mmol/L

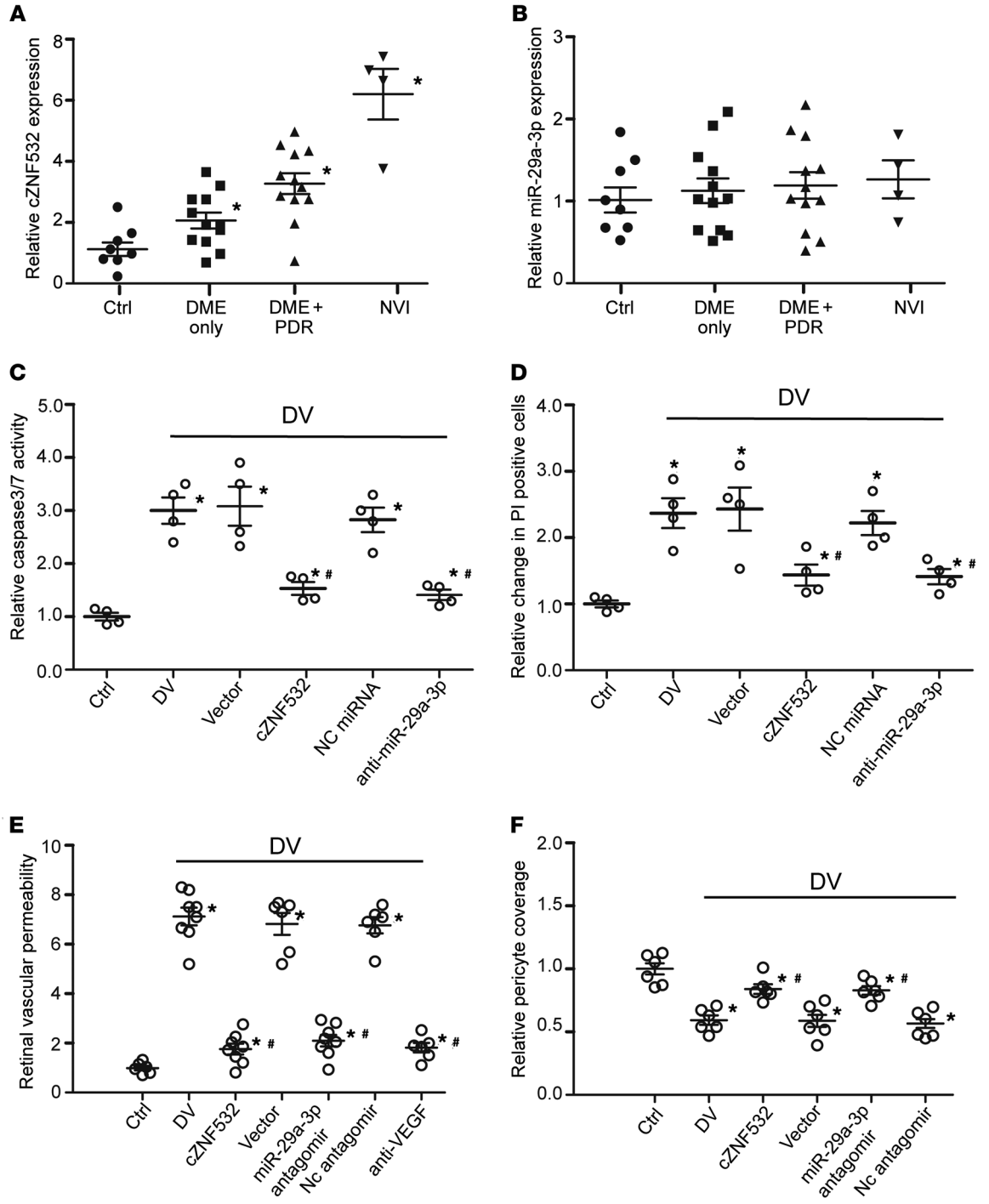

Figure 7. Clinical implication of cZNF532/miR-29a-3p/NG2, LOXL2, and CDK2 signaling in retinal vascular dysfunction. (**A** and **B**) Human vitreous specimens were obtained from 36 subjects at the time of pars plana vitrectomy, including non-DR samples (Ctrl, n = 8 eyes) and those from patients with DME only (n = 12 eyes), DME with PDR (n = 12 eyes), and NVI (n = 4 eyes). qRT-PCR was conducted to detect the expression of cZNF532 (**A**) and miR-29a-3p (**B**) in vitreous samples. *P < 0.05 versus Ctrl group, Kruskal-Wallis's test followed by Bonferroni's post hoc test. (**C** and **D**) Pericytes were transfected with cZNF532 overexpression vector (cZNF532), null vector (Vector), anti–miR-29a-3p, or negative control miRNA for 24 hours or left untreated, and then incubated without (Ctrl) or with 50 μL diabetic vitreous (DV) for 24 hours. Cell apoptosis was detected by caspase-3/7 activity (**C**, n = 4) or PI staining (**D**, n = 4). *P < 0.05 versus Ctrl group, #P < 0.05 versus DV group. One-way ANOVA followed by Bonferroni's post hoc test. (**E**) EB evaluation of retinal vasopermeability in retinal extracts from mice injected with PBS (Ctrl, n = 6), diabetic vitreous without (DV, n = 8) or with cZNF532 overexpression vector (cZNF532, n = 8), null vector (Vector, n = 6), miR-29a-3p antagomir (n = 8), negative control (NC, n = 6) antagomir, or anti-VEGF (n = 6) after 1 week of treatment. (**F**) Pericyte coverage was quantified by staining the whole-mount retinas with IB4 and NG2 from the mice after intravitreal injection of PBS (Ctrl, n = 6) diabetic vitreous without (DV, n = 6) or with cZNF532 overexpression vector (cZNF532, n = 6), null vector (Vector, n = 6), miR-29a-3p antagomir (n = 6), or NC (n = 6) antagomir 1-week after treatment. The statistical result was shown. *P < 0.05 versus Ctrl group, #P < 0.05 versus DV group, Kruskal-Wallis's test followed by Bonferroni's post hoc test. Error bar indicates SD.

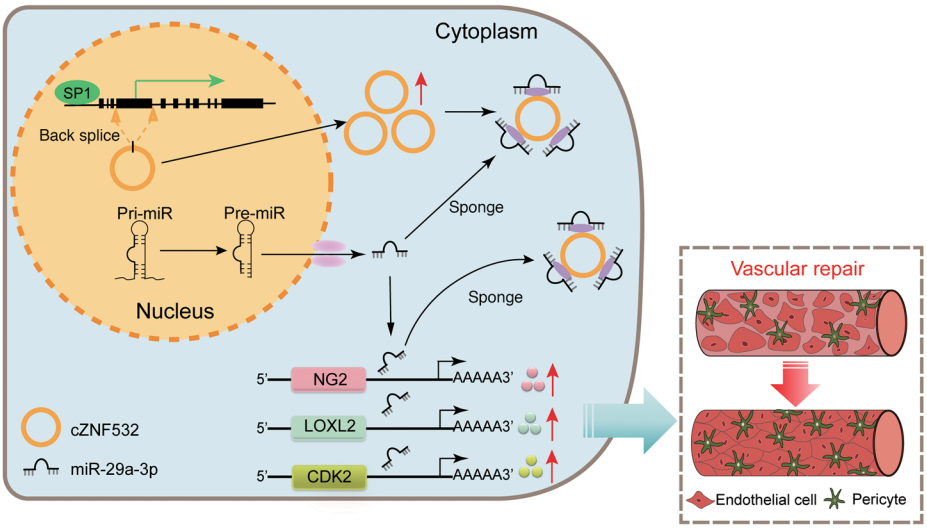

Figure 8. Model of cZNF532 function and mechanism in retinal vascular dysfunction. cZNF532, an important regulator of pericyte function and vascular homeostasis, protects against diabetes-induced retinal pericyte degeneration and vascular dysfunction by acting as a miR-29a-3p sponge to sequester and inhibit miR-29a-3p activity, inducing increased expression of NG2, LOXL2, and CDK2.

D-glucose concentration supplemented with 10% fetal bovine serum (FBS, Gibco, 11573397) and cell growth supplements. They were incubated at 37°C, 5% CO_2, and 95% relative humidity. HRVECs (passage 4–7) were cultured in EGM2-MV medium supplemented with 5% FBS at 5.55 mmol/L D-glucose concentration. High glucose concentrations were obtained by adding D-glucose to a final concentration of 30 mmol/L. These cells were transfected at approximately 80% confluence using Lipofectamine RNAiMax (Life Technologies, 13778150) or Lipofectamine 3000 (Life Technologies, L3000015) according to the manufacturer's protocols.

Animals and STZ-induced diabetic retinopathy. Wild-type C57BL/6J mice were purchased from Nanjing Qinglongshan Experimental Animal Center (Nanjing, China). PDGFR-β-Cre mice were purchased from Beijing Biocytogen Co. Ltd (Beijing, China) generated on the pure C57BL/6J background. DR was induced by intraperitoneal injection of STZ (MilliporeSigma, 572201). WT mice (8 weeks old, male) or PDGFR-β-Cre mice (8 weeks old, male) were fasted for 6 hours before STZ injection. They received STZ (50 mg/kg in 10 mM citrate buffer, pH 4.5) injection for 5 consecutive days. Control mice were administered sodium citrate buffer. All mice were bred in an air-conditioned room with a 12-hour light-dark cycle. They were fed with standard laboratory chow and allowed free access to water. Seven days later, the blood from the tail vein was used for the measurement of glucose level by OneTouch Ultra meter (LifeScan). The mice with a blood glucose level of over 300 mg/dL were deemed diabetic.

Circular RNA microarray. Human retinal pericytes we incubated with 5.55 mM glucose (n = 3, NG), 5.55 mM glucose plus 24.45 mM pyruvate (n = 3, OS), or 30 mM glucose (n = 3, HG) for 24 hours, and then prepared RNA samples for circRNA expression profiles. Circular RNA microarray arrays were conducted by commercial microarray (4 × 180 K, Human Circular RNA Microarray; Shanghai Biotechnology Co. Ltd.) with a total of 88,371 probes. In brief, total RNAs were incubated with RNAse R to eliminate linear RNAs. The enriched circRNAs were amplified, transcribed into fluorescent cRNAs, and purified by the RNeasy Mini Kit (Qiagen, 74104). The Cy3-labeled cRNAs were hybridized onto Circular RNA Microarrays by the Gene Expression Hybridization Kit (Agilent Technologies, 5188-5242) at 65°C for 16 hours. After washing, the signal of the Circular RNA Microarray was scanned by the Agilent Microarray Scanner (Agilent Technologies).

Retinal trypsin digestion assay. Retinal vasculature was isolated by trypsin digest method. Briefly, the mouse eye was enucleated and fixed in 4% paraformaldehyde for 24 hours. The retina was dissected under a microscope and washed with water for 30 minutes at least 4 or 5 times. Retina was incubated in a solution of 3% trypsin (1:250, BD Difco, 215250) in 0.1 M Tris buffer (pH 7.8) at 37°C for approximately 1.5 hours when the tissue began showing the sign of disintegration. After trypsin digestion, retina was gently shaken to free vessel network, washed, and mounted on glass slides. Retinal vasculature was stained with periodic acid-Schiff hematoxylin (PAS-hematoxylin) and observed under a light microscopy. The number of acellular capillaries, microaneurysms, and pericyte ghosts was counted in 15 to 20 randomly selected fields (×400 magnification) in the mid-retina in a masked manner, which was standardized to capillary area (per mm^2 capillary area).

Intravitreal injection. C57BL/6 mice (8 weeks old, male) were anesthetized through the intraperitoneal injection of ketamine (80 mg/kg) and xylazine (4 mg/kg). A 33-gauge disposable needle was passed through the sclera at the equator and posterior to the limbus into the vitreous cavity. Approximately 1.5 μL adeno-associated virus or miRNA inhibitor/mimic was subsequently injected into the vitreous cavity with direct observation of the needle directly above the optic nerve head. The adeno-associated virus was used in 1×10^{12} vg/mL titers. There was about a 1- to 2-week delay in the conversion of recombinant adeno-associated virus DNA to a transcriptionally active double-stranded form. The adeno-associated virus was thus injected 2 weeks before diabetes induction.

Quantification of pericyte coverage. The whole-mount mouse retinas were used for pericyte coverage detection by immunofluorescence staining. The eyes were enucleated and fixed in 4% paraformaldehyde (Biosharp Biotechnology, BL539A) in PBS (pH 7.5) for 30 minutes at room temperature. The eyes were then transferred to cold 1 × PBS on ice for 5 to 10 minutes. The neural retina and choroid/RPE were dissected separately and placed in cold formaldehyde. Retinas were then blocked in 1% Triton-X/5% BSA for 30 minutes. The whole-mount retina was stained with NG2 (1:100, Abcam, ab50009) overnight at 4°C and Alexa Fluor 594 goat anti–mouse IgG (1:500, Invitrogen,

A11005) for 3 hours at room temperature to label pericytes. The retinas were then stained with Isolectin B4 (GS-IB4, 1:100, MilliporeSigma, L2895) for 2 hours at room temperature to label endothelial cells. Fluorescence images were acquired using an IX73P1F fluorescence microscope (Olympus). Pericyte coverage was quantified using Image J software to measure the length of GS-IB4$^+$ vessel associated with NG2$^+$ pericyte process. Direct contact between pericytes (NG2) and endothelial cells (GS-IB4) were detected by the colocalization analysis with BioImage XD.

Evans blue assay. Retinal capillary permeability was determined by EB assay. EB dye covalently linked to albumin was used as an indicator of albumin leakage into the retina from the capillary. Briefly, the mice were anesthetized using intraperitoneal ketamine (80 mg/kg) and xylazine (4 mg/kg). EB dye (100 mg/mL, MilliporeSigma, E2129) was dissolved in PBS and sonicated for 20 minutes and filtered (pore size, 0.22 μm). EB dye was injected into the femoral vein at the dosage of 45 mg/kg and the blood samples were collected. After the dye circulated for 1 to 2 hours, the chest cavity was opened. The mice were perfused with citrate buffer (0.05 M, pH 3.5). After perfusion, the eyes were enucleated and bisected at the equator. For immunofluorescence observation, the eyes were fixed in 4% paraformaldehyde for 30 minutes at room temperature. After removing the cornea, lens, and vitreous body, the retina was carefully removed from choroid and sclera. The retinal cups were cut radically to lie flat. *Z*-stack images were captured through a ×10 objective. For quantitative assessment, the retinas were dissected from the eyeballs. After the measurement of retinal wet weight, the retinas were dried for 5 hours. EB dye conjugated to serum albumin in retinas was extracted by solubilization in formamide (0.2 mL per retina) at 78°C overnight. The resulting suspensions were placed in an ultracentrifuge at 120,000*g* at 4°C for 45 minutes. EB dye in the supernatant was spectrophotometrically detected by absorbance at 620 nm (blue signal) and 740 nm (background subtracted). Blood samples were treated similarly but without solubilization. They were centrifuged at 3600*g* at 25°C for 15 minutes. The concentration of EB dye was calculated from a standard curve of EB dye in formamide and normalized to dry retina weight. Retinal vascular leakage was calculated using the equation: (retinal EB, μg / retinal dry weight, mg) / (time averaged EB concentration, μg / plasma, μl × circulation time, h). Dry weight was substituted for wet weight, with results being expressed in microliter plasma retinal dry weight $mg^{-1}\ h^{-1}$.

Statistics. Data were tested for normality by the Pearson normality test and for the homogeneity of variances by the Levene test. Continuous data were expressed as mean ± SD. For in vivo data, each *n* value corresponds to a single mouse. For in vitro data, each *n* value corresponds to an independent experiment. If technical replicates were conducted, their mean was considered as $n = 1$. No statistical method was used to predetermine sample size that was based on preliminary data. All available data were included and no data were excluded from analysis. For normally distributed data with equal variance, the difference was determined by 2-tailed Student *t* test (2-group comparisons) or 1-way or 2-way ANOVA followed by Bonferroni's post hoc test (multigroup comparisons) as appropriate. For nonnormally distributed data or data with unequal variances, the difference was determined by the nonparametric Mann-Whitney *U* test (2-group comparisons) or Kruskal-Wallis test followed by Bonferroni's post hoc test (multigroup comparisons). A *P* value of less than 0.05 was considered statistically significant. GraphPad Prism 8 and Microsoft Excel 2016 were used for all calculations. The circRNA microarray data for the identification of high glucose–regulated circRNAs in pericytes was deposited in the NCBI's Gene Expression Omnibus (GEO) database (GSE14367).

Study approval. Animal experiments were conducted in accordance with the Association for Research in Vision and Ophthalmology Statement for the Use of Animals in Ophthalmic and Vision Research and approved by the Animal Care and Use Committee of Eye and ENT Hospital and Nanjing Medical University. The surgical specimens were handled according to the Declaration of Helsinki. The clinical protocols were approved by the institutional review committee of Nanjing Medical University and Eye and ENT Hospital.

See Supplemental Methods online for additional methods.

Author contributions

BY, CZ, and QJ designed the research studies. BY, CL, CPL, SSX, MDY, HMG, YNS, XML, SJZ, KS, and BHL conducted the experiments and acquired and analyzed data. BY wrote the manuscript. QJ and JY provided advice. All authors critically reviewed the manuscript.

Acknowledgments

This work was funded by the grants from the National Natural Science Foundation of China (81770945 and 81970809 to BY, 81570859 to QJ, and 81670878 to JY), and a grant from the Shanghai Youth Talent Support Program (to BY).

Address correspondence to: Biao Yan, Fudan University, 83 Fen Yang Road, Shanghai, China 200030. Phone: 86.21.64377134; Email: yanbiao1982@hotmail.com. Or to: Qin Jiang, Nanjing Medical University, 138 Han Zhong Road, Nanjing, China 200090. Phone: 86.25.86677677; Email: jqin710@vip.sina.com. Or to: Chen Zhao, Fudan University, 83 Fen Yang Road, Shanghai, China 200030. Phone: 86.21.64377134; Email: dr_zhaochen@163.com.

1. Geevarghese A, Herman IM. Pericyte-endothelial crosstalk: implications and opportunities for advanced cellular therapies. *Transl Res*. 2014;163(4):296–306.
2. Armulik A, Abramsson A, Betsholtz C. Endothelial/pericyte interactions. *Circ Res*. 2005;97(6):512–523.
3. Bischoff FC, et al. Identification and functional characterization of hypoxia-induced endoplasmic reticulum stress regulating lncRNA (HypER-lnc) in Pericytes. *Circ Res*. 2017;121(4):368–375.
4. Stark K, et al. Capillary and arteriolar pericytes attract innate leukocytes exiting through venules and 'instruct' them with pattern-recognition and motility programs. *Nat Immunol*. 2013;14(1):41–51.
5. Hall CN, et al. Capillary pericytes regulate cerebral blood flow in health and disease. *Nature*. 2014;508(7494):55–60.
6. Selvam S, Kumar T, Fruttiger M. Retinal vasculature development in health and disease. *Prog Retin Eye Res*. 2018;63:1–19.
7. Shenoy AK, et al. Epithelial-to-mesenchymal transition confers pericyte properties on cancer cells. *J Clin Invest*. 2016;126(11):4174–4186.
8. Mollazadegan K, Ludvigsson JF. Diabetes: Microvascular complications in T1DM and coeliac disease. *Nat Rev Endocrinol*. 2015;11(6):320–322.
9. Forbes JM, Cooper ME. Mechanisms of diabetic complications. *Physiol Rev*. 2013;93(1):137–188.
10. Antonetti D. Eye vessels saved by rescuing their pericyte partners. *Nat Med*. 2009;15(11):1248–1249.
11. Motiejūnaite R, Kazlauskas A. Pericytes and ocular diseases. *Exp Eye Res*. 2008;86(2):171–177.
12. Flammer J, Konieczka K, Bruno RM, Virdis A, Flammer AJ, Taddei S. The eye and the heart. *Eur Heart J*. 2013;34(17):1270–1278.

13. Mizutani M, Kern TS, Lorenzi M. Accelerated death of retinal microvascular cells in human and experimental diabetic retinopathy. *J Clin Invest*. 1996;97(12):2883–2890.
14. Pfister F, et al. Pericyte migration: a novel mechanism of pericyte loss in experimental diabetic retinopathy. *Diabetes*. 2008;57(9):2495–2502.
15. Wang Q, et al. Low-dose erythropoietin inhibits oxidative stress and early vascular changes in the experimental diabetic retina. *Diabetologia*. 2010;53(6):1227–1238.
16. Caporarello N, et al. Pericytes in microvessels: from "mural" function to brain and retina regeneration. *Int J Mol Sci*. 2019;20(24):E6351.
17. Lasda E, Parker R. Circular RNAs: diversity of form and function. *RNA*. 2014;20(12):1829–1842.
18. Huang S, et al. The emerging role of circular RNAs in transcriptome regulation. *Genomics*. 2017;109(5-6):401–407.
19. Chen LL. The biogenesis and emerging roles of circular RNAs. *Nat Rev Mol Cell Biol*. 2016;17(4):205–211.
20. Shao Y, Chen Y. Roles of circular RNAs in neurologic disease. *Front Mol Neurosci*. 2016;9:25.
21. Chen Y, Li C, Tan C, Liu X. Circular RNAs: a new frontier in the study of human diseases. *J Med Genet*. 2016;53(6):359–365.
22. McKenzie JA, et al. Apelin is required for non-neovascular remodeling in the retina. *Am J Pathol*. 2012;180(1):399–409.
23. Majumdar G, Wright J, Markowitz P, Martinez-Hernandez A, Raghow R, Solomon SS. Insulin stimulates and diabetes inhibits O-linked N-acetylglucosamine transferase and O-glycosylation of Sp1. *Diabetes*. 2004;53(12):3184–3192.
24. Liu C, et al. Targeting pericyte-endothelial cell crosstalk by circular RNA-cPWWP2A inhibition aggravates diabetes-induced microvascular dysfunction. *Proc Natl Acad Sci USA*. 2019;116(15):7455–7464.
25. Yamaguchi H, de Lecea L. In vivo cell type-specific CRISPR gene editing for sleep research. *J Neurosci Methods*. 2019;316:99–102.
26. Armulik A, Genové G, Betsholtz C. Pericytes: developmental, physiological, and pathological perspectives, problems, and promises. *Dev Cell*. 2011;21(2):193–215.
27. Pagano M, et al. Regulation of the cell cycle by the cdk2 protein kinase in cultured human fibroblasts. *J Cell Biol*. 1993;121(1):101–111.
28. Payne SL, et al. Lysyl oxidase regulates breast cancer cell migration and adhesion through a hydrogen peroxide-mediated mechanism. *Cancer Res*. 2005;65(24):11429–11436.
29. Gao BB, et al. Extracellular carbonic anhydrase mediates hemorrhagic retinal and cerebral vascular permeability through prekallikrein activation. *Nat Med*. 2007;13(2):181–188.
30. García C, et al. Vasoinhibins prevent retinal vasopermeability associated with diabetic retinopathy in rats via protein phosphatase 2A-dependent eNOS inactivation. *J Clin Invest*. 2008;118(6):2291–2300.
31. Stitt AW, et al. The progress in understanding and treatment of diabetic retinopathy. *Prog Retin Eye Res*. 2016;51:156–186.
32. Hammes HP, et al. Pericytes and the pathogenesis of diabetic retinopathy. *Diabetes*. 2002;51(10):3107–3112.
33. Majumdar G, Wright J, Markowitz P, Martinez-Hernandez A, Raghow R, Solomon SS. Insulin stimulates and diabetes inhibits O-linked N-acetylglucosamine transferase and O-glycosylation of Sp1. *Diabetes*. 2004;53(12):3184–3192.
34. Sharma I, Dutta RK, Singh NK, Kanwar YS. High glucose-induced hypomethylation promotes binding of sp-1 to myo-inositol oxygenase: implication in the pathobiology of diabetic tubulopathy. *Am J Pathol*. 2017;187(4):724–739.
35. Cai J, Boulton M. The pathogenesis of diabetic retinopathy: old concepts and new questions. *Eye (Lond)*. 2002;16(3):242–260.
36. Barber AJ, Gardner TW, Abcouwer SF. The significance of vascular and neural apoptosis to the pathology of diabetic retinopathy. *Invest Ophthalmol Vis Sci*. 2011;52(2):1156–1163.
37. Bennett J. Taking stock of retinal gene therapy: looking back and moving forward. *Mol Ther*. 2017;25(5):1076–1094.
38. Nicolosi PA, Dallatomasina A, Perris R. Theranostic impact of NG2/CSPG4 proteoglycan in cancer. *Theranostics*. 2015;5(5):530–544.
39. Sweeney MD, Ayyadurai S, Zlokovic BV. Pericytes of the neurovascular unit: key functions and signaling pathways. *Nat Neurosci*. 2016;19(6):771–783.
40. Nishikawa R, et al. Tumour-suppressive microRNA-29s directly regulate LOXL2 expression and inhibit cancer cell migration and invasion in renal cell carcinoma. *FEBS Lett*. 2015;589(16):2136–2145.
41. Lolli G, Johnson LN. CAK-cyclin-dependent activating kinase: a key kinase in cell cycle control and a target for drugs? *Cell Cycle*. 2005;4(4):572–577.
42. Wu JH, et al. Inhibition of Sema4D/PlexinB1 signaling alleviates vascular dysfunction in diabetic retinopathy. *EMBO Mol Med*. 2020;12(2):e10154.
43. Amoaku WM, et al. Defining response to anti-VEGF therapies in neovascular AMD. *Eye (Lond)*. 2015;29(6):721–731.
44. Wang H, Feng L, Hu J, Xie C, Wang F. Differentiating vitreous proteomes in proliferative diabetic retinopathy using high-performance liquid chromatography coupled to tandem mass spectrometry. *Exp Eye Res*. 2013;108:110–119.